# District heating by drinking water heat pump: Modelling and energy analysis of a case study in the city of Milan

A.M. De Pasquale [a, 1], A. Giostri [a, *, 1], M.C. Romano [a, 1], P. Chiesa [a, 1], T. Demeco [b], S. Tani [b]

[a] Politecnico di Milano e Dipartimento di Energia, Via Lambruschini 4, 20156 Milano, Italy
[b] Metropolitana Milanese (MM), Via del Vecchio Politecnico, 8, 20121 Milano, Italy

This paper investigates the integration of a district heating heat pump for the production of about 4.65 $MW_{th}$ with the drinking water networkeplaying the role of low temperature heat source -as an alter-native to conventional fossil fuel heating. The heat recovery reduces water temperature from 15 °C to 12 °C, thus requiring partial reheating by the drinking water end-user that needs to be estimated to evaluate the energetic convenience of this solution. Heat transfer between water mains and surrounding soil is considered by a proper thermal model computing the temperature vs. time profile at nodes. The developed model, which exploits Epanet to simulate the water network, compares the primary energy consumption and $CO_2$ emissions of the studied system with a conventional district heating solution. Each component, which constitute the overall system, (i.e. heat pump, water network, heating by water end-user etc.) is analyzed and modelled. Assuming a fossil fuel based scenario, the investigated heat pump system reduces the overall primary energy consumption and $CO_2$ emission by about 3%. This value boosts to 41% in case all the electricity generation relies on renewables, thus proving this solution is a promising alternative to conventional district heating in future energy scenarios dominated by renewables.

***Keywords:*** Energy efficiency, Drinking water heat recovery, Heat pump, District heating

## 1. Introduction

In order to mitigate air pollution and global warming, different solutions have been considered involving the reduction of fossil fuels consumption [1]. Focusing on municipal environment, cities can be identified as a sort of "climate change industry" [2,3] and, in particular, heating demand is recognized as one of the most important fields that deserves dedicated actions to mitigate the contribution to climate change.

This study analyses an option to reduce primary energy consumption for district heating in urban scenario through the replacement of conventional centralized boilers with heat pump systems. In particular, heat pump is recognized as a valuable alternative that can be more efficient -from a thermodynamic point of view- than traditional district heating systems based on fossil fuel combustion. In addition, the increase of thermal load covered by heat pumps can facilitate the management of electricity network in scenarios characterized by a high fraction of electricity from intermittent renewable energy sources. As a matter of fact, heat pumps could act as an interface between electrical and thermal networks in municipal smart grids, that are recognized as systems able to overcome the challenges implied by the fluctuating nature of electricity from renewable sources [4].

The first opportunity to integrate heat pumps in municipal environment and exploit existing resources is represented by the extraction of heat from waste water. It is estimated that, in residential areas, about 60% of the drinking water provided is heated, used as hot water and then discharged in the sewage system. The thermal energy loss (i.e. the residual thermal energy in discharged water from shower) is about the 15% of the global heat provided to the user (included space heating) [5]. In Ref. [6] it is estimated that, in a residential building, the average temperature of the discharged water is about 27 °C. On a small scale, it is possible to apply heat pumps that use the waste water collected in the sewer of a building as heat source. This is the case of a hospice in Switzerland, where a 30 kW heat pump is installed [5]. On a larger scale, the heat recovery process can directly involve sewage systems and waste water treatment plants. It is possible to apply heat pumps that extract thermal energy from the sewage water and make it available at higher temperature. For example, in Oslo about 8% of

*Article history:*
Received 19 July 2016
Received in revised form
14 November 2016
Accepted 4 December 2016

* Corresponding author.
*E-mail address:* andrea.giostri@polimi.it (A. Giostri).
[1] www.gecos.polimi.it.


Published Journal Article available at: http://dx.doi.org/10.1016/j.energy.2016.12.014

**Acronyms**

| | |
|---|---|
| COP | Coefficient of performance |
| DAE | Differential algebraic equation |
| HP | Heat pump |
| HVAC | Heating ventilation and air conditioning |
| IGV | Inlet guides vane |
| IRR | Internal rate of return |
| MM | Metropolitana Milanese |
| NPV | Net present value |
| NG | Natural gas |
| ST | Storage tank |

*Nomenclature*

| | |
|---|---|
| C | Generic integration constant, – |
| $c_p$ | Specific heat, J $kg^{-1}$ $K^{-1}$ |
| D | Diameter, m |
| d | Burying depth, m |
| E | Energy, J |
| F | $CO_2$ emission factor, $g_{CO2}$ $kWh^{-1}$ |
| h | Convective heat transfer coefficient, W $m^{-2}$ $K^{-1}$ |
| k | Thermal conductivity, W $m^{-1}$ $K^{-1}$ |
| l | Additional soil layer thickness, m |
| LHV | Lower heating value, MJ $kg^{-1}$ |
| m | Mass flow, kg $s^{-1}$ |
| M | Mass, kg |
| P | Pressure, Pa |
| Q | Thermal energy, J |
| $\dot{Q}$ | Thermal power, W |
| $\dot{q}$ | Specific heat transfer rate, W $m^{-1}$ |
| S | Shape factor, – |
| T | Temperature, °C |
| t | time, s |
| U | Overall heat transfer coefficient, W $m^{-2}$ $K^{-1}$ |
| W | Electric power, W |
| x | x-coordinate, m |
| y | y-coordinate, m |

*Subscripts*

| | |
|---|---|
| A | Case A |
| B | Case B |
| compr | compressor |
| cond | condenser |
| DH | District heating |
| dom | domestic |
| el | electric |
| eva | Evaporator |
| f | fluid |
| in | inlet |
| mech | mechanical |
| NG | Natural gas |
| O | Initial state |
| off | Off-design |
| on | On-design |
| out | Outlet |
| p | Pipe |
| pp | Pinch point |
| prim | primary |
| ref | reference |
| RH | Reheating |
| SC | Sub-cooling |
| SH | Super-heating |
| ST | Storage tank |
| th | thermal |
| US | User |

*Superscripts*

| | |
|---|---|
| s | Superficial |
| t | Time varying |
| u | Undisturbed |

*Greek letters*

| | |
|---|---|
| Δ | Difference, – |
| α | Drinking water fraction to be heated, – |
| χ | Heat fraction, – |
| η | Efficiency, – |
| ρ | Density, kg $m^{-3}$ |
| ω | Angular frequency, $s^{-1}$ |

thermal energy required by district heating is obtained by recovering heat from the sewage system [7]. A similar system was installed near the Olympic village in Vancouver [8,9]. Heat recovery downstream of water treatments (where large flows and stable temperatures are observed) is applied in about 20 cites in Switzerland. For example, in the Bremgarten quarter in Berna about 60% of the heat demand is provided by heat pumps that extract thermal energy from treated water [5].

Another thermal energy resource in cities is represented by the drinking water that constantly flows throughout the distribution network. This resource shows a vast potential in terms of exploitable thermal energy.

Few studies concerning heat recovery from drinking water are available in the literature. Compared to waste water, potable water generally has lower temperatures that penalize the energetic performance of heat pumps. However, there are many factors in favor of the use of the water supply system as heat source for heat pumps, namely: i) the increase of drinking water temperature in the distribution network can lead to bacteria growth, with consequent risks for users' health [7], ii) compared to the case of a geothermal heat pump using ground water, there is no significant increase of costs linked to the pumping of the fluid (since these are already included in the management of the aqueduct), iii) there is no need of additional drillings of aquifer and the risk of ground water pollution is limited, iv) compared to the case of a heat pump using waste water, fouling problems of the heat exchanger are much less significant and v) water mass flow is more stable than wastewater one, thus simplifying the heat pump operation.

In this paper the opportunity to use a heat pump that exploits drinking water as cold heat source is analyzed. The impact that this solution can have on end-users of the water service is assessed, considering that they receive cooler water and thus an additional heating is requested to maintain the same utilization temperature. The analysis both considers the energetic and the environmental aspect, by assessing primary energy balance and $CO_2$ emissions. The case study refers to a district of Milan, whose characteristics are provided by Metropolitana Milanese (MM) that is the municipal utility that manages the water service.

With the aim of evaluating the system performance, a tailored-made model, whose characteristics are discussed in the following sections, is developed. In particular, it is worth underlining that the developed model maintains a high level of flexibility that allows its

use in other cities or in context different from the residential one (e.g. industrial area).

## 2. General analysis of the system

The main concepts considered in this paper can be introduced by a simplified analysis of the energy flows of a district-heating system designed to meet the thermal energy requirements of a hypothetical residential user. The conventional system (Case A) is compared to a heat pump integrated with the drinking water network (Case B). Fig. 1 shows a block-scheme representation reporting both the energy and water flows.

Case A adopts a centralized fossil-fueled heater that converts a part of the primary energy input ($E_{prim,A}$) associated to fossil fuel (i.e. natural gas) into heat provided to the end-users ($Q_{US}$), with a conversion efficiency equal to $\eta_{th}$. Case B takes into account an electricity-driven heat pump (HP) that moves thermal energy ($Q_{eva}$) from a cold sink, which is represented by drinking-water network, to the hot water sink distributed to the end-users ($Q_{US}$). Electricity consumed by the heat pump derives from a power generation system converting primary energy input ($E_{prim,el,B}$) into electricity with an efficiency equal to $\eta_{el}$. It is worth underlining that the district heating users are a subset of residential users; as a matter of fact, drinking water is distributed to the whole residential customers, whereas thermal energy is delivered only to a fraction of the drinking water customers.

In Case B, the extraction of heat from drinking water causes a temperature drop that implies an additional thermal load ($Q_{RH}$) – reheating "RH"- that has to be provided by each user connected to the drinking water system. $Q_{RH}$ is assumed to be provided by natural gas fired boilers located at the end user. Here, the water is taken to the same temperature of Case A, consuming primary energy $E_{prim,heater,B}$ dependent on the efficiency of the distributed heaters.

The study of this system cannot be conducted without considering the heat transfer between soil and drinking water mains that can be positive or negative depending on the relative temperature of soil and water. Heat exchanged between water and soil is termed as $Q_{soil}$, assumed positive when soil is colder than water. As an example in a typical winter condition characterized by soil colder than drinking water, water cooling caused by the heat pump reduces the heat transfer between water and surrounding soil. The difference between $Q_{soil}$ in Case A and B is expressed as a fraction ($\chi$) of the thermal energy extracted from water ($Q_{eva}$). This effect contributes reducing the thermal load for water reheating.

It is worth noticing that only a fraction ($\alpha$) of drinking water needs to be heated up by the end user (e.g. washing machine, cooking, shower, etc.), whereas the remaining fraction bypasses the heating system (e.g. toilet water) and does not need any further heating.

As an example, please consider that in case A drinking water enters the network at the same temperature measured at wells outlet (15 °C). Because of the heat transfer with a colder soil ($Q_{soil,A}$), drinking water cools down by certain $\Delta T_{soil,A}$, reaching a temperature $T_{user,A}$ at the entrance of user home. In Case B, temperature at water network inlet is 12 °C, as a consequence of the 3 °C cooling due to the heat pump. The modification of heat transfer driving force (i.e. the temperature difference between water and soil) involves a reduction of the heat transferred to the surrounding soil that is lower than in Case A. As a result, temperature of water distributed to the user ($T_{user,B}$) is lower than temperature in Case A but the difference is less than 3 °C because of the different $Q_{soil}$. $Q_{RH}$ is represented by the primary energy spent by the user of drinking water service to bring back up the fraction $\alpha$ of the distributed drinking water to a temperature equal to $T_{user,A}$.

In order to quantify the difference of primary energy consumption between Case B and Case A ($\Delta E_{prim}$), a mathematical relation, which takes into account the main parameters, can be derived as follows.

$$\Delta E_{prim} = E_{prim,B} - E_{prim,A} = \left(E_{prim,el,B} + E_{prim,heater,B}\right) - E_{prim,A} = \left(\frac{E_{el,compr}}{\eta_{el}} + \frac{Q_{RH}}{\eta_{th}}\right) - \frac{Q_{US}}{\eta_{th}} \quad (1)$$

The heat pump coefficient of performance (COP) is defined as

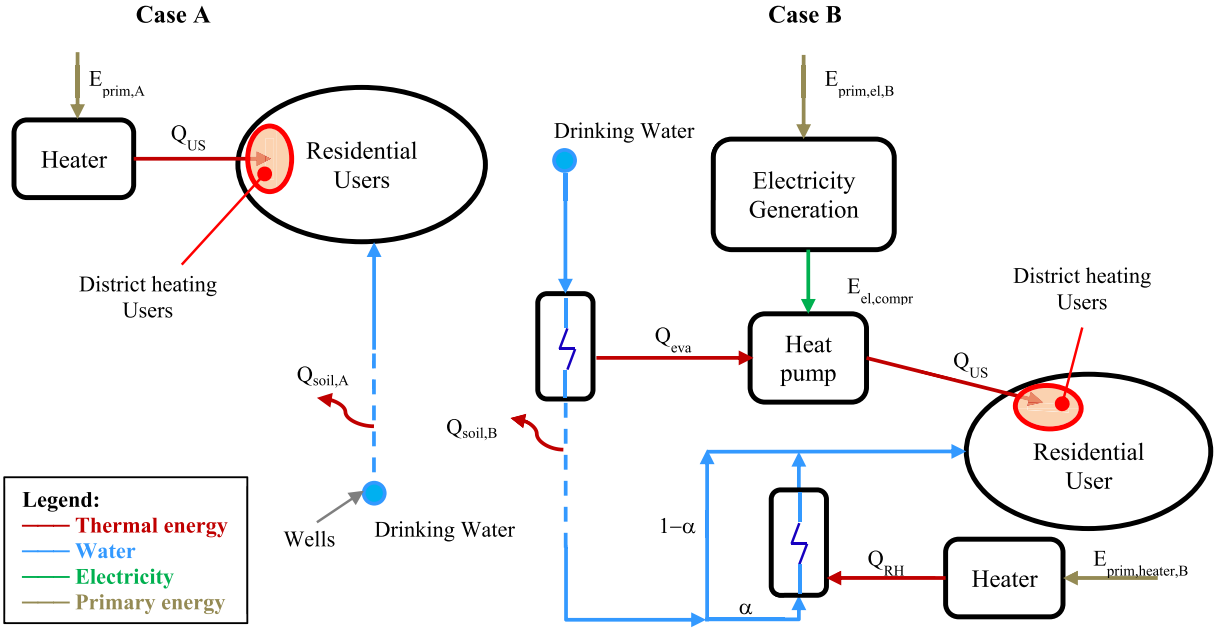


**Fig. 1.** Blocks scheme of the studied system. Nomenclature and main subsystems considered in the preliminary analysis are reported. In addition, the district heating user, as a subset of drinking water user, is highlighted.

the ratio between the thermal energy delivered to users ($Q_{US}$) and the electricity consumption necessary to drive the compressor ($E_{el,compr}$):

$$COP = \frac{Q_{US}}{E_{el,compr}} \tag{2}$$

The heat extracted from the drinking water by the evaporator of the heat pump ($Q_{eva}$) can be expressed as a function of $Q_{US}$ and COP, by the following equation:

$$\begin{aligned} Q_{eva} &= Q_{US} - E_{fluid,compr} = Q_{US}\left(1 - \frac{E_{el,compr} \cdot \eta_{el-mech,compr}}{Q_{US}}\right) \\ &= Q_{US}\left(\frac{COP - \eta_{el-mech,compr}}{COP}\right) \end{aligned} \tag{3}$$

where $E_{fluid,compr}$ is the energy transferred by compressor to HP working fluid and $\eta_{el-mech,compr}$ is the conversion efficiency from electricity to compressor shaft power.

With the aim of expressing the reheating energy ($Q_{RH}$) as function of the district heating demand ($Q_{US}$), the COP, $\alpha$ and $\chi$, it is possible to write:

$$\begin{aligned} Q_{RH} &= \alpha\left[Q_{eva} - \left(Q_{soil,A} - Q_{soil,B}\right)\right] = \alpha Q_{eva}(1-\chi) \\ &= Q_{US}\left(\frac{COP - \eta_{el-mech,compr}}{COP}\right)\alpha(1-\chi) \end{aligned} \tag{4}$$

Based on the relations expressed in Equations (2)–(4), Equation (1) can be rearranged to the following final form, where all the main parameters are made explicit.

$$\Delta E_{prim} = Q_{US}\left(\frac{1}{COP\eta_{el}} - \frac{1}{\eta_{th}} + \frac{\alpha(1-\chi)\left(COP - \eta_{el-mech,compr}\right)}{COP\eta_{th}}\right) \tag{5}$$

The relation expressed by Eq. (5) captures the effect on primary energy consumption of the main system parameters: COP, $\alpha(1-\chi)$ fraction, $\eta_{el,compr}$, $\eta_{el}$ and $\eta_{th}$. Condition with $\chi$ equal to 1 represents an ideal condition in which water from cold heat sink does not need any reheating by end-users ($Q_{RH}$ equal to zero), thus leading to the highest primary energy gain implied by the switch from Case A to Case B. $\alpha$ equal to unity stands for a condition where the total user water demand needs to be heated. Fig. 2 offers a graphical representation of Eq. (1) outlining the effect of the parameters that influence the difference of primary energy $\Delta E_{prim}$ consumption between the two investigated solutions (values are normalized by $Q_{US}$). In general, high COP, high $\eta_{el}$, low $\eta_{th}$ and low $\alpha(1-\chi)$ favors Case B with respect to Case A.

As stated previously, this preliminary discussion aims at giving an indicative view of the main parameters affecting the overall energy balance of the assessed system. The effect of the parameter $\chi$, which is dependent on the thermal interaction between water pipes and soil can play a significant role. Therefore, in the following sections, a model for the estimation of this interaction is presented, in order to properly evaluate the overall energy performance of the illustrated system.

## 3. System modelling

It is possible to identify five sub-components that constitute the overall system of Case B (Fig. 3): i) a wells field from which drinking water is extracted by dedicated pumps, ii) a thermal station that comprises a heat pump connected with the main water pipe and an auxiliary boiler placed in parallel, iii) a pumping station made up of a storage tank and pumps that distribute the water to the municipal network, iv) the drinking-water network, consisting of nodes (i.e. users or junctions) and pipes and v) the district heating network.

In the following, the modelling approach and the assumptions related to each component are described and discussed.

### 3.1. Water wells

Water mass flow extracted from underground wells is assumed to be constant with time. Water temperature can also be assumed to be constant with time according to geographical region and wells depth. In this study, the temperature is assumed equal to 15 °C. Direct temperature measurements (available from a single well with a depth of 100 m) show slight oscillations along the year (about 1 °C) that, as a first approximation, lead to consider water temperature as constant. No thermal interaction between water and surroundings is considered along the pipes connecting the wells to the main station. The validity of the last assumption is verified in case the studied system is placed near water extraction wells and, consequently, the connecting pipes length is small.

### 3.2. Thermal station

Thermal load requested by district heating is provided by a dedicated thermal station made up of a heat pump (HP) and an auxiliary natural gas (NG) heater placed in parallel. The heat pump is sized in order to fulfill base load, while the auxiliary heater operates to cover demand peaks or very low thermal loads, below the minimum load of the heat pump (assumed corresponding to 35% of the design load in this study). A by-pass branch allows controlling the water mass flow rate processed by the heat pump in order to fulfill the time profile of thermal load. It has to be remarked that this simple connection is not the optimal one from the energy efficiency point of view. As a matter of fact, the alternative connection with HP and NG heater in series would allow reducing the water temperature at the HP condenser outlet and therefore the condensation temperature, with beneficial effects on the COP. However, the effects of such a configuration would be limited on a yearly balance (about 2–3% of HP electric energy saving for the case study of this paper), as further discussed in Sec. 3.5.

Water temperature sent to the district heating network is set to 80 °C, while return water temperature is assumed equal to 65 °C. The chosen temperatures can be considered as indicative of the existing district heating networks in Milan, where buildings are heated by high temperature systems (e.g. radiator) and the heating network also fulfills sanitary water demand. A continuous action control on the water mass flow rate is assumed, keeping a constant outlet temperature in any operating conditions. An alternative control criterion may be to keep a constant water mass flow rate and reduce the temperature of the heated water at low loads. Such control logic would be more efficient because the heat pump condensing temperature can be reduced at low loads, with beneficial effects on the COP. However, this control approach would require proper modelling of the thermal behavior of the buildings connected to the district heating network, to provide the relation between thermal load and water temperatures. Moreover, it would require additional non-standard auxiliary local control units, to manage the non-uniform heat load variation of the different users. As a matter of fact, the mismatch of heat load between different users connected to the same district heating network (for example because of different building insulations and variable solar radiation) would require the distribution of water with different temperatures for the different users instead of the standard system where different flow rates of water with the same temperature are

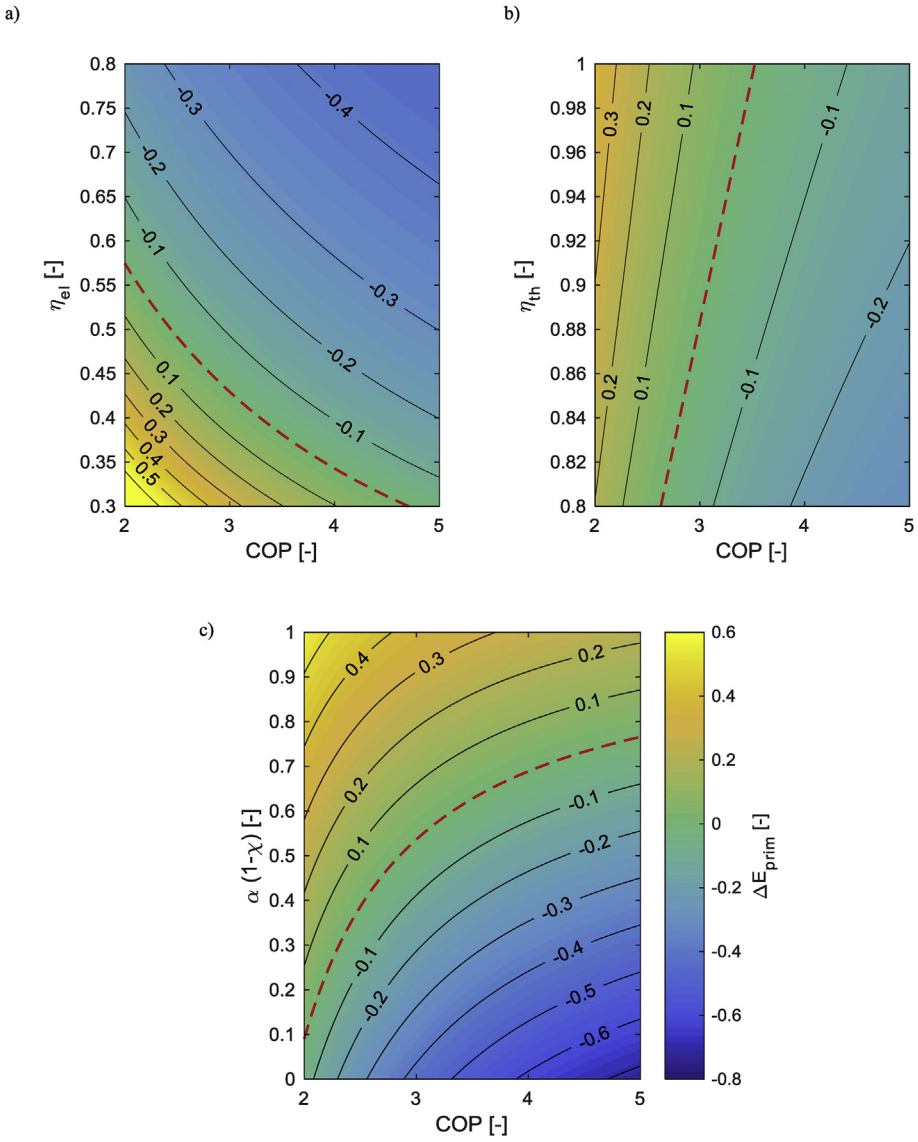


**Fig. 2.** Effect of COP, $\eta_{el}$ (a), $\eta_{th}$(b) and $\alpha(1-\chi)$ (c) on $\Delta E_{prim}$. $\Delta E_{prim}$ equal to zero are represented by red-dashed line. Negative value represents an energy save of Case B over Case A. Reference values of $\eta_{el}$, $\eta_{th}$, $\alpha(1-\chi)$ and $\eta_{el\text{-}mech}$ in charts where these effects are not assessed, are 0.446, 0.85, 0.5 and 0.98 respectively. (For interpretation of the references to colour in this figure legend, the reader is referred to the web version of this article.)

distributed to the users.

### 3.2.1. Heat pump

The two-stage vapor compression cycle with flash (refrigerant fluid R134a) is currently recognized as one of the best solutions to comply with heat load of the order of few MW with a temperature level of 80 °C [10].

Fig. 4 shows the layout of the modelled two-stage heat pump with both the stream numbers and component names reported. Stream 1 represents the compressor suction state. R134a vapor is compressed by the low-pressure compressor stage (C1). Saturated vapor exiting the flash (FL) is mixed with the fluid processed by the low-pressure compressor (C1) and enters the high pressure compressor (C2). Compressed flow (stream 4) is sent to the condenser (COND) where it successively is desuperheated, condensed and subcooled (stream 5). Water mass flow (stream 12) is heated up in the condenser and sent to the district heating (stream 13) at the desired temperature. The subcooled liquid (with a $\Delta T_{SC}$ of 2 °C) enters the high pressure expansion valve (EX2) through which it expands (stream 6) and enters the flash. Stream 8 is the flashed vapor, which is mixed in mixer (MX) with stream 2 from compressor C1, whereas stream 7 is saturated liquid that is expanded through the low-pressure expansion valve (EX1). In the evaporator (EVA), flash mixture is evaporated and slightly superheated ($\Delta T_{SH}$ of 3 °C) to generate the compressor suction flow (stream 1). The water from the drinking water network is cooled down from condition 10 to condition 11, assuming a temperature drop of 3 °C (i.e. from 15 °C to 12 °C).

As suggested in Ref. [10], the part-load operation is handled by compressor inlet guide vanes (IGV) down to 45% of the design thermal load, whereas at lower load the hot gas bypass (HGB) (dashed circuit in Fig. 4) diverts a part of the flow from compressor C2 directly to the evaporator, bypassing the condenser. The minimum HP thermal load is set to 35% of the design load. Below this threshold the heat pump is shut down. It is worth noticing that the adoption of variable speed driver control coupled with IGV could be a valuable solution to increase COP in part-load. Nevertheless, this control type is not considered in the present study in order to be

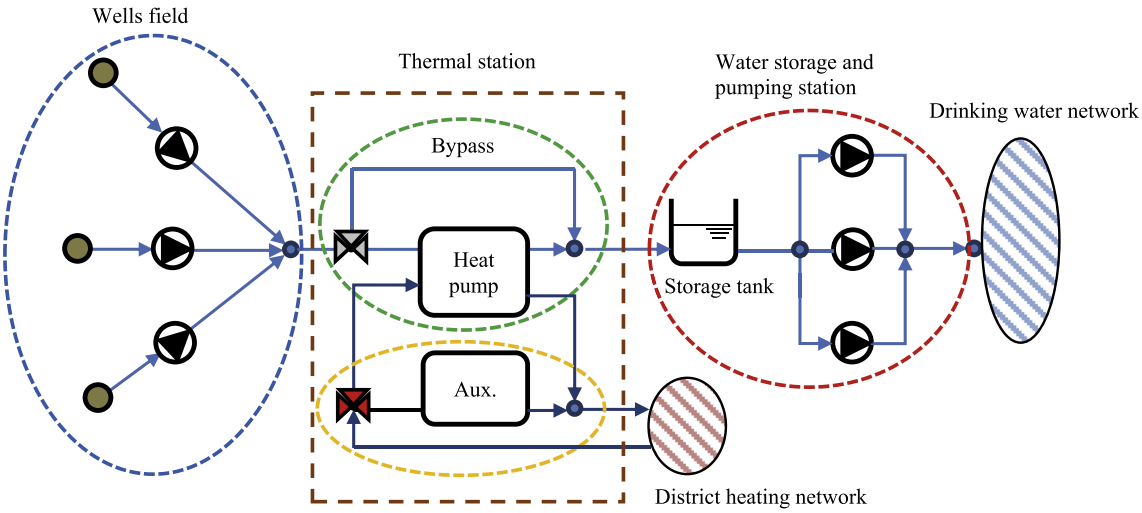


**Fig. 3.** Simplified scheme of the studied system, indicating the five subcomponents modelled in this work.

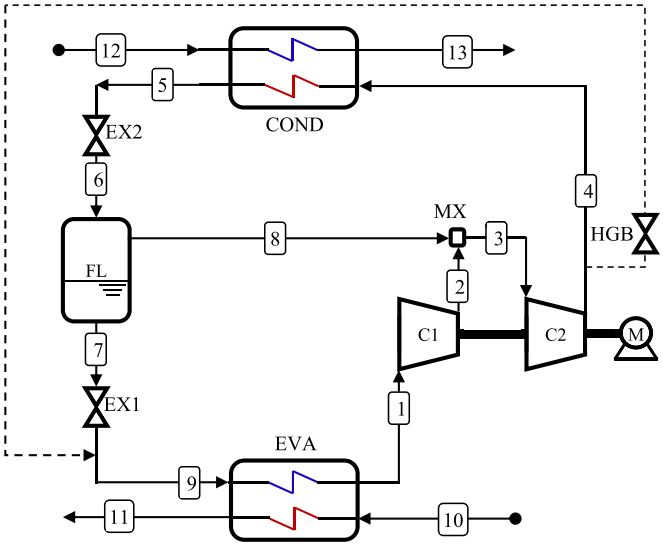


**Fig. 4.** Two-stage vapor compression cycle.

consistent with the reference manufacturer technology [10].

Thermoflex® (TFX) [11] has been used to model the heat pump and to compute both on-design and part-load performance.

The main assumptions for the components design, compatible with selected heat pump technology, are reported in Table 1. As regards the heat pump capacity, it is defined by the thermal power required by the district heating, as further discussed in Section 3.5. The COP obtained from the model shows a good agreement with real heat pump model available on the market [10].

It is important to remark that the chosen sizing assumptions are not derived from a rigorous economic optimization but they can be considered representative of considered HP size. It is recognized by the authors that the optimization of the heat pump design parameters, which should result from the trade-off between operating and investment costs, would augment the attractiveness of the proposed system. Nevertheless, it is reasonable to expect that the main conclusions of this work are not strongly affected by the lack of such a rigorous HP design optimization.

To take into account the effects of the thermal load change, the part-load performance of heat pump has been calculated. In order to predict the compressor behavior, compressor map presented in Ref. [12] is considered and isentropic efficiency of both stages is obtained through interpolation. E-Link® toolkit capabilities are exploited to enable communication between TFX and an Excel® worksheet that handles compressor efficiency calculation.

Fig. 5 reports the COP change as function of the load. Three characteristic zones can be identified. At high loads (from 100% to 85% the design load approximately), it occurs a small change in COP, that maintains close to the design value. This effect is caused by the trade-off between the decrease of compressor isentropic efficiency, operating in off-design conditions, and the increase of the effectiveness of the heat exchangers that result in a decrease of the condensation temperature and an increase of the evaporation one. At middle loads (from 85% to 45% of the design thermal load), the reduction of COP, which falls to a value of 2.5, is evident. This is due to the prevalent effect of compressor efficiency reduction with respect to the increase of the heat exchanger effectiveness. At low loads (below 45%), the switch from IGV control to hot gas bypass leads to a steep decrease of COP down to about 2 at 35% of the design thermal load, that represents the minimum operation limit of the heat pump.

#### 3.2.2. Auxiliary heater

A natural gas fired auxiliary heater is considered in this study. A thermal efficiency of 90% on low heating value (LHV) basis is assumed, independently of the load.

### 3.3. Water storage and pumping station

Once drinking water is processed by the heat pump, it is sent to a storage tanks (ST) that serve as buffer storage between the constant water flow rate extracted from the wells and the variable water flow in the drinking water network, which depends on the demand of the end users. In order to compute the stored mass and the temperature inside the tank vs. time, two main assumptions have been made: the storage tank model is assumed to be adiabatic and perfectly mixed (i.e. at each time water temperature distribution is uniform). Mass and energy conservation laws are therefore expressed in differential form by Eqs. (6) and (7).

$$\frac{dM_{ST}}{dt} = m_{in,ST} - m_{out,ST} \tag{6}$$

**Table 1**
Heat pump model assumptions and performance at the design point.

| | Symbol | Value | Unit of measurement |
|---|---|---|---|
| Heat Pump design point assumptions | | | |
| Refrigerant name | – | R134a | – |
| Isentropic efficiency of low pressure compressor C1 | $\eta_{is,C1}$ | 85.0 | % |
| Isentropic efficiency of low pressure compressor C2 | $\eta_{is,C2}$ | 85.0 | % |
| Compressor mechanical efficiency | $\eta_{mech\text{-}comp}$ | 99.0 | % |
| Electric motor efficiency | $\eta_{motor}$ | 96.86 | % |
| Condensation pressure | $P_5$ | 27.50 | bar |
| Condensation temperature | $T_{COND}$ | 82 | °C |
| Flash pressure | $P_7$ | 8.81 | bar |
| Evaporator pressure | $P_9$ | 3.5 | bar |
| Evaporation temperature | $T_{EVA}$ | 5 | °C |
| District heating hot water temperature | $T_{13}$ | 80 | °C |
| District heating cold water temperature | $T_{12}$ | 65 | °C |
| District heating water mass flow rate | $m_{12}$ | 74.07 | kg $s^{-1}$ |
| Water temperature at evaporator inlet | $T_{10}$ | 15 | °C |
| Water temperature at evaporator outlet | $T_{11}$ | 12 | °C |
| Evaporator superheating | $\Delta T_{SH}$ | 3 | °C |
| Condenser subcooling | $\Delta T_{SC}$ | 2 | °C |
| Heat Pump design point performance | | | |
| Compressor electrical power | $W_{compr}$ | 1515.6 | $kW_e$ |
| Evaporator thermal power | $\dot{Q}_{eva}$ | 3200 | $kW_t$ |
| Condenser thermal power | $\dot{Q}_{cond\ cond}$ | 4653 | $kW_t$ |
| Coefficient of Performance | COP | 3.003 | – |

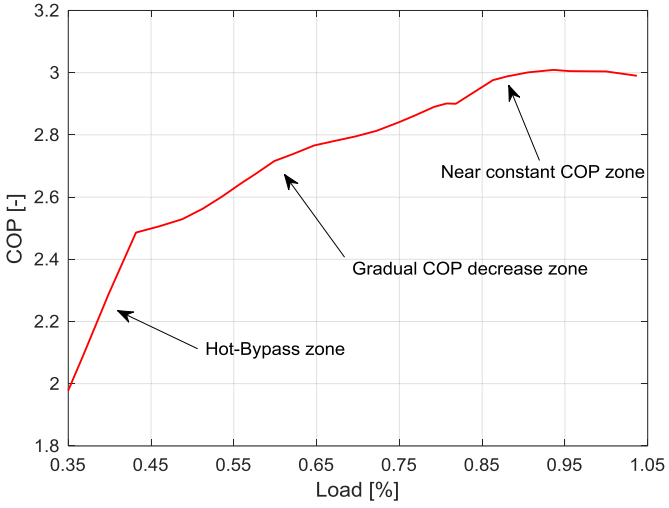


**Fig. 5.** Heat pump COP-load map.

$$\frac{d(M_{ST}c_pT_{ST})}{dt} = m_{in,ST}c_pT_{in,ST} - m_{out,ST}c_pT_{out,ST} \tag{7}$$

where M is the water mass contained in the storage tanks and $c_p$ is specific heat of water.

Considering thermophysical water properties as temperature independent in the conditions relevant for this work, for time intervals with constant $T_{in,ST}$, $m_{in,ST}$ and $m_{out,ST}$, an analytical solution exists to calculate the water mass contained in the tank (Eq. (8)) and the temperature of the water leaving the tank (Eq. (9)). The equations include the initial temperature $T_{0,ST}$ and initial mass $M_{0,ST}$ in the storage tanks.

$$M_{ST}(t) = M_{0,ST} + (m_{in,ST} - m_{out,ST})t \tag{8}$$

$$\begin{cases} if\ \ m_{in,ST} = m_{out,ST} \\ T_{out,ST}(t) = T_{in,ST} + (T_{0,ST} - T_{in,ST})e^{-\frac{m_{in,ST}}{M_{0,ST}}t} \\ if\ \ m_{in,ST} \neq m_{out,ST} \\ T_{out,ST}(t) = T_{in,ST} + C_1\left[C_2 + (m_{in,ST} - m_{out,ST})t\right]^{\frac{m_{in,ST}}{m_{out,ST}-m_{in,ST}}} \end{cases} \tag{9}$$

where:

$$C_1 = (T_{0,ST} - T_{in,ST})M_{0,ST}^{\frac{m_{in,ST}}{m_{in,ST}-m_{out,ST}}} \tag{10}$$

$$C_2 = M_{0,ST} \tag{11}$$

Water temperature inside the storage tank is the same of the drinking water that is pumped and delivered to the consumers. Water temperature change through the pumps is neglected. Electric consumption of the pumps is not considered in the energy balance, being invariant in the two cases assessed in this work.

### 3.4. Drinking water distribution network

Water network is a crucial component of the studied system characterized by a high complexity. As underlined in section 2, not only water flow distribution (hydraulic problem) but also water temperature (thermal problem) is fundamental to estimate the energetic impact of replacing a central boiler district heating with a heat pump.

#### 3.4.1. Pipe thermal model

As described in previous sections, the thermal behavior of a buried water pipe has to be assessed in order to estimate the effect of the heat recovery of water sent to customers through the drinking water network. In this section, four different models are described and compared with the aim of identifying the approach

that best suits the modelling requirements in terms of both accuracy and computational resources.

The investigated system is made up of a single water pipe that is ground buried at a depth of 1.5 m. The problem is characterized by a bi-dimensional geometry.

Thermophysical properties of both water and soil are assumed to be constant. In particular, because of the small temperature changes, the first assumption does not lead to any significant uncertainty, whereas the dependence of soil thermophysical properties (e.g. density, thermal conductivity and specific heat capacity) on temperature, composition and water content (i.e. water infiltration) [13] could be a source of uncertainty that is neglected in this study.

*3.4.1.1. Finite element model (FEM).* The simulation of a buried pipe can be approached through a finite elements method as shown in Ref. [14]. In this work the commercial software Comsol® 5.0 [15] is used for these calculations. The system is studied as a 2D transient model and the system geometry is approximated by a rectangular domain, which represents the soil, with a circle representing the pipe outer wall. In order to reduce the computational efforts, the convective heat transfer between water and tube wall is modelled as a Cauchy boundary condition, with the well-established Dittus-Boelter correlation [16] for convective heat transfer. In this way, the solution of the thermo-fluid-dynamic problem inside the pipe is avoided. In Fig. 6a, the geometry and the generated mesh are shown. Fine mesh around the pipe is requested in order to accurately capture the temperature disturbance caused by pipe. Although the soil domain is finite (20 m height and 20 m width), the thermal behavior can be approximated accurately by the semi-infinite medium one (see Appendix).

Boundary conditions at the bottom and left side of domain are adiabatic while, in order to reduce mesh size and consequently computational time, a symmetry boundary condition is applied on the right hand side of the domain. A sinusoidal temperature time profile, defined in the Appendix, is imposed at domain top surface.

FEM model is able to compute the spatial temperature profile for each time, as shown in Fig. 6b, and to compute heat transfer between the pipe and the surrounding soil. Simulated time is longer than one year in order to stabilize the solution that depends on the

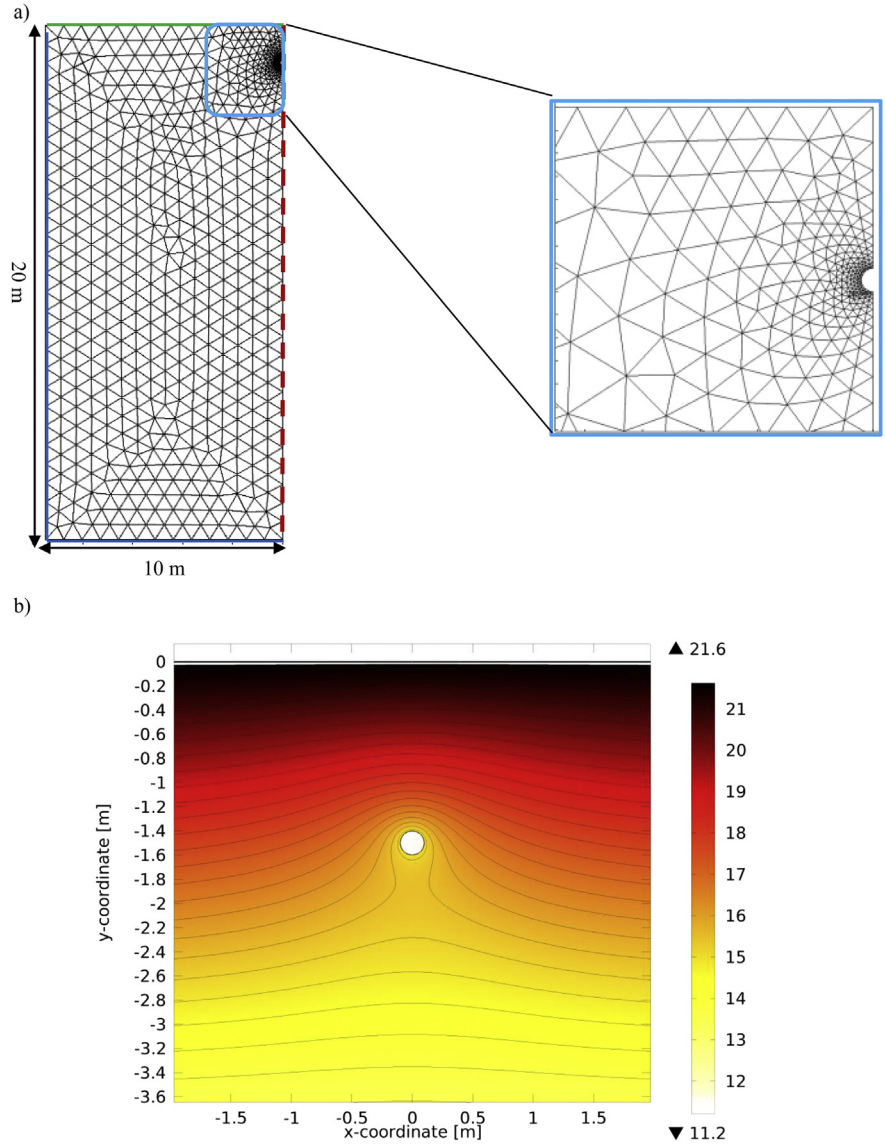


**Fig. 6.** Analyzed geometry with zoom (light blue) of zone near the pipe (a). Boundary conditions are: i) symmetry (dashed red), ii) adiabatic (blue) and iii) imposed temperature (green). Temperature profile (expressed in °C) at 13-Aug 6:00 a.m. for a buried depth of 1.5 m and pipe diameter equal to 0.2 m. Soil temperature diffusivity equal to 6.48e−7 $m^2 s^{-1}$ (see Appendix). (For interpretation of the references to colour in this figure legend, the reader is referred to the web version of this article.)

initial condition (i.e. uniform temperature). It is worth noticing that a 2D finite element model does not need any information about the soil temperature profile because it is solved directly once soil properties and surface temperature time profile are defined.

*3.4.1.2. Analytical models.* Although the FEM model is characterized by a high level of accuracy, the high computational resources needed leads to consider the adoption of simplified thermal models that can predict heat transfer between drinking water pipe and the surrounding soil with proper accuracy but reduced computational time. In particular, FEM model computes the temperature distribution in the domain that is unnecessary for the scope of this study where only the heat transfer between the pipe and the soil is needed. In the following sections, three simpler analytical models from literature are reported and compared.

*3.4.1.2.1. Undisturbed soil model.* Only two studies, which deal with the thermal behavior of water mains, are present in literature [17,18]. Both these models implement the same thermal model where the outer wall pipe temperature is assumed equal to the undisturbed soil temperature at the burying depth ($T^u_{soil}$) (see Appendix) and the overall heat transfer coefficient depends on conduction through pipe wall and convection of the flowing water. With this model, the overall heat transfer coefficient (referred to the outer tube area) is computed as follows[2]:

$$UA = \frac{1}{\frac{1}{\pi D_{in} h_{conv}} + \frac{\ln(D_{out}/D_{in})}{2\pi k_{pipe}}} \tag{12}$$

where $D_{in}$ and $D_{out}$ stand for the inner and outer diameter of the pipe respectively, $h_{conv}$ is the convective heat transfer coefficient (computed with Dittus-Boelter's correlation [16]) and $k_{pipe}$ is the thermal conductivity of pipe wall.

The heat transfer rate ($\dot{q}$ [W m$^{-1}$]), specific to the pipe length, is computed as follows:

$$\dot{q} = UA(T_{water} - T^u_{soil}) \tag{13}$$

*3.4.1.2.2. Shape factor.* Another modelling approach considers that the system can be represented as an isothermal infinite cylinder buried in a semi-infinite medium with surface temperature imposed. In this case, conduction in the surrounding soil has to be added to the thermal resistance network considered by the undisturbed soil model [19]. The overall heat transfer coefficient (referred to as the outer tube area) is computed as follows:

$$UA = \frac{1}{\frac{1}{\pi D_{in} h_{conv}} + \frac{ln(D_{out}/D_{in})}{2\pi k_{pipe}} + \frac{1}{k_{soil} S}} \tag{14}$$

The shape factor (S) takes into accounts the two-dimensional heat transfer occurring in the soil with thermal conductivity $k_{soil}$. S depends on the geometrical characteristics of the studied configuration as underlined in Ref. [19] and, in case of infinite length cylinder buried in a semi-infinite medium, it is analytically expressed per unit length of cylinder as follows:

$$S = \frac{2\pi}{cosh(2d/D_{out})} \tag{15}$$

where d is the piping burying depth.

[2] In the original publication, the overall heat transfer coefficient is expressed as referred to a planar geometry instead of a cylindrical one. Taking into account the characteristic dimension of the system, this assumption does not add any significant errors.

Heat transfer rate, specific to pipe length, is computed with the same relation of the undisturbed soil model after substituting the undisturbed soil temperature $T^u_{soil}$ with the ground superficial temperature $T^s_{soil}$.

$$\dot{q} = UA(T_{water} - T^s_{soil}) \tag{16}$$

*3.4.1.2.3. Krarti-Kreider's model.* With the aim of approximating the thermal disturbance caused by pipe on surrounding soil temperature, Krarti and Kreider developed a specific model [20].

Although the proposed model was originally developed to study heat transfer in underground air tunnel, it can be considered suitable to study the heat transfer in drinking water main with the adoption of small changes. This model represents a middle ground between the FEM and the steady-state model previously described. In the Krarti-Kreider's model, dynamic effect induced by seasonal variation of ambient temperature on a buried water pipe are taken into account. The disturbance added by the buried pipe on the surrounding soil is modelled by superimposing the thermal behavior of the pipe on the undisturbed soil temperature. This goal is reached through the addition of a fictitious soil layer with thickness l, which is function of the thermophysical soil properties and the angular frequency ($\omega$) of the ground surface sinusoidal function (see Appendix) as expressed in Eq. (17). The effect of this additional layer is ultimately an increase of the system thermal resistance.

$$l = \sqrt{\frac{\left(\frac{k}{\rho c_p}\right)_{soil}}{\omega}} \tag{17}$$

Fig. 7 shows the parameters that are considered in Krarti-Kreider's model, with reference to both a longitudinal and cross section of the system.

Heat flux is evaluated by applying conduction/convection equations between the all the interfaces as reported in Eq. (18):

$$\dot{q} = h_{conv}\pi D_{in}\left(T_{water} - T^{pipe}_{in}\right) = 2\pi \frac{k_{pipe}}{ln\left(\frac{s_{pipe}+\frac{D_{in}}{2}}{\frac{D_{in}}{2}}\right)}\left(T^{pipe}_{in} - T^{pipe}_{out}\right)$$
$$= 2\pi \frac{k_{soil}}{ln\left(\frac{l+\frac{D_{in}}{2}+s_{pipe}}{\frac{D_{in}}{2}+s_{pipe}}\right)}\left(T^{pipe}_{out} - T^{u}_{soil}\right) = U_s\pi D_{in}\left(T^{pipe}_{in} - T^{u}_{soil}\right) \tag{18}$$

where $T^u_{soil}$ is the undisturbed soil temperature, $T^{pipe}_{in}$ stands for temperature at inner surface of pipe, $T^{pipe}_{out}$ is the outer pipe wall temperature and $s_{pipe}$ is the pipe wall thickness. All these temperatures are time dependent.

$U_s$, which represents the overall heat transfer coefficient of the pipe wall material and additional soil layer, is computed as follows:

$$U_s = \frac{\left(\frac{2}{D_{in}}\right)}{\frac{1}{k_{soil}} ln\left(\frac{l+\frac{D_{in}}{2}+s_{pipe}}{\frac{D_{in}}{2}+s_{pipe}}\right) + \frac{1}{k_{pipe}} ln\left(\frac{s_{pipe}+\frac{D_{in}}{2}}{\frac{D_{in}}{2}}\right)} \tag{19}$$

*3.4.1.3. Models comparison.* A comparison between the four models described, in terms of heat transfer per unit length of buried pipe, has been undertaken, as shown in Fig. 8, in order to assess their suitability for modelling of the system. All the models predict maximum heat fluxes approximately in the range 20–30 W m$^{-1}$, with the exception of the undisturbed soil model that computes a

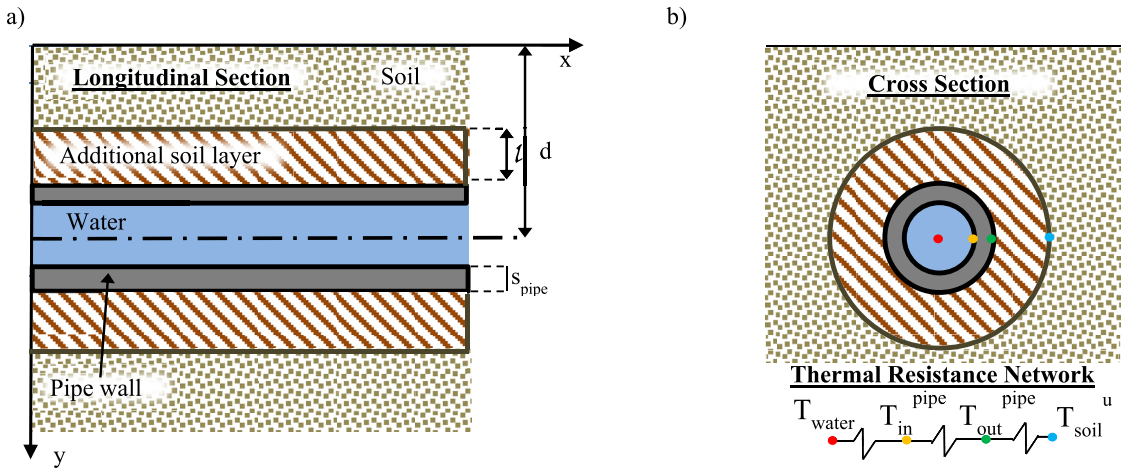


**Fig. 7.** Longitudinal section of buried pipe with parameters considered by Krarti's model (a). Cross section with characteristic temperature and equivalent thermal resistance network reported (b).

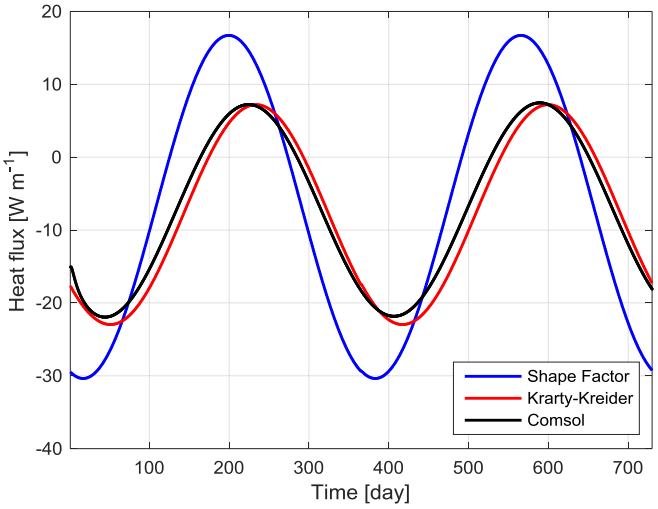


**Fig. 8.** Comparison among different models based on heat flux per unit of pipe length. Burial depth and pipe diameter are equal to 1.5 m and 0.2 m respectively. Water temperature is equal to 15 °C. Ground temperature profile vs. time is reported in the Appendix.

thermal power two orders of magnitude higher than other models (and is therefore excluded from Fig. 8). This effect is a direct consequence of neglecting the thermal disturbance of the pipe on the surrounding soil, by assuming the pipe wall temperature equal to the undisturbed soil temperature. The oscillating trend of the heat flux in Fig. 8 derives from the ground temperature profile discussed in the Appendix. A negative heat flux represents a condition characterized by soil colder than water, while a positive heat flux denotes that water is heated by the surrounding soil.

As regards the shape factor model, the main difference is related to the absence of any time delay between the ambient temperature and the heat flux temporal profile.

A comparison between Krarti-Kreider's model and the Comsol® model enlightens an excellent agreement of the heat flux profiles. Therefore, the Krarti-Kreider's model, thanks to its accuracy coupled with reduced computational efforts, is selected to be implemented in the study.

Although the undisturbed soil model is identified as unsuitable to model a buried pipe, a comparison with the implemented model is useful to underline the effect of the thermal model on water temperature prediction along a pipe. In addition, it is worth noticing that the undisturbed soil model was implemented in the two studies found in literature dealing with the energetic assessment of a system similar to the one investigated in this work [17,18]. Hence, a comparison with the Krarti-Kreider's model can show the quantitative effect of choosing different thermal models. For this purpose, water temperature is computed along pipe length of 1000 m.

As described in the previous section, the overall heat transfer coefficient is constant and uniform along the pipe that, together with the assumption of water and soil properties independent of temperature, allows finding an analytical solution (Eq. (20)) of water temperature profile along the pipe:

$$T(t) = T^u_{soil} - (T^u_{soil} - T_0)e^{\frac{-4U_{tot}t}{\rho_{soil}c_{p_{soil}}D}} \quad (20)$$

Fig. 9 shows the water temperature along the pipe computed with undisturbed soil model and Krarti-Kreider's model in case of undisturbed soil temperature equal to 5.71 °C. Two cases, characterized by different pipe material, namely black iron (Fig. 9a) and PVC (Fig. 9b), are reported. The comparison between the two figures points out how the two models predict dissimilar temperature profiles. In case of high conductive pipe material, the difference is particularly large, because most of the thermal resistance is imputable to soil layer, which is neglected by the undisturbed soil model. As a consequence, heat transfer is highly overestimated in this case. The reduction of thermal conductivity implied by PVC (0.42 W $m^{-1}$ $K^{-1}$) and the related thermal resistance leads to a reduced difference between two models caused by the reduction of the weight of soil layer resistance on the total heat transfer coefficient.

*3.4.1.4. Parametric analysis.* Because a municipal drinking water network is made up of different pipe segments characterized by different diameter, materials and water mass flow rates, a simple parametric analysis is conducted in order to estimate the effect of these parameters on the temperature profile along a 1000 m long pipe (Eq. (20)). In accordance with the previous analysis, the undisturbed soil temperature is assumed equal to 5.71 °C. The conducted parametric analysis is summarized in Table 2.

The first studied parameter is the pipe material that affects the pipe thermal conductivity in Eq. (19). Cast iron, concrete and PVC have a thermal conductivity of 55, 1 and 0.42 W $m^{-1}$ $K^{-1}$ respectively. Despite the big difference of the thermal conductivity of the

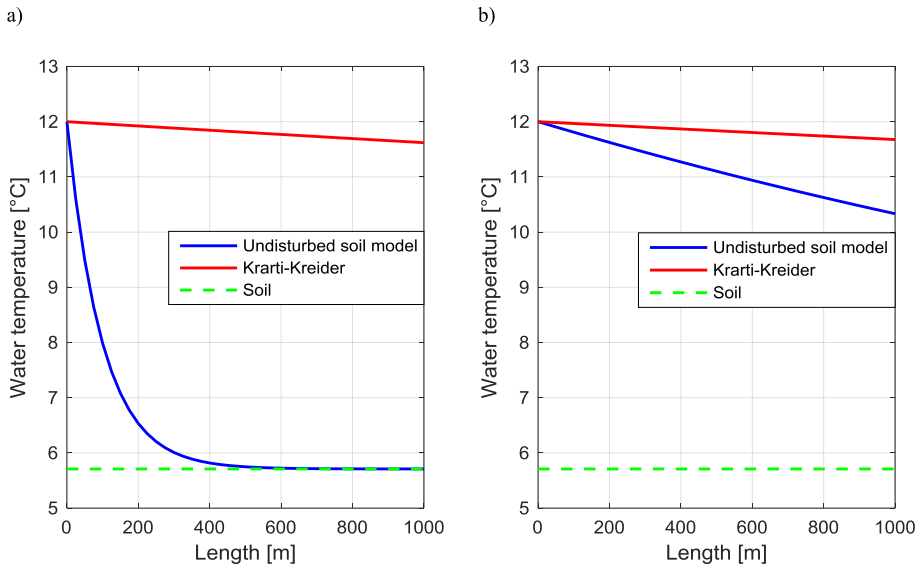


**Fig. 9.** Comparison between spatial temperature profile computed by undisturbed soil model and Krarti-Kreider's model for cast iron ($k_{pipe}$ = 55 W m$^{-1}$ K$^{-1}$) (a) and PVC pipe ($k_{pipe}$ = 0.42 W m$^{-1}$ K$^{-1}$) (b). Green dashed line represents the soil temperature at 1.5 m depth. Pipe inner diameter is 0.2 m ($s_{pipe}$ = 0.02 m) and pipe length is 1000 m. Water volume flow is equal to 10 l s$^{-1}$. Undisturbed soil temperature and water inlet temperature are 5.71 °C and 12.0 °C respectively. (For interpretation of the references to colour in this figure legend, the reader is referred to the web version of this article.)

**Table 2**
Investigated parameters in the parametric analysis. In accordance with [21], pipe thickness is assumed 10% of inner pipe diameter.

| Parameter | Pipe material | Pipe diameter [mm] | Mass flow [kg s$^{-1}$] |
|---|---|---|---|
| Pipe material | Cast iron-Concrete-PVC | 150 | 10 |
| Pipe diameter | Cast iron | 100–400 (step 100) | 10 |
| Mass flow rate | Cast iron | 300 | 10–40 (step 10) |

considered pipe materials, the total heat transfer coefficient is dominated by soil layer and, as shown in Fig. 10a, the outlet temperature is slightly influenced by the pipe material.

An increase of the pipe diameter implies a reduction of the overall heat transfer coefficient both directly and indirectly (through the increase of wall thickness) as shown in Eq. (19). Nevertheless, the higher the pipe diameter, the higher the water temperature change (Fig. 10b), as consequence of the higher heat transfer surface.

The last investigated parameter is the water mass flow rate. In this case, the higher the mass flow rate, the smaller the temperature change as shown in Fig. 10c. Although the increase of the mass flow rate leads to higher convective heat transfer coefficient, its effect is negligible on the global heat transfer coefficient. As a consequence, the temperature difference between inlet and outlet reduces when the mass flow rate increases.

### 3.4.2. Hydraulic model

In order to have a more complete view of the investigated problem, the thermal model has to be coupled with the hydraulic model of the drinking water network. First, the drinking water network has to be physically defined including network topology that comprises nodes position and pipe characteristics (i.e. length, diameter, roughness, elevation etc.). As reported in the introduction, this study considers a portion of the Milan network made up of 1195 nodes and 1366 pipes, whose characteristics are supplied by the Milan drinking water service utility MM. Pipe material of the studied network is mainly metallic. In particular, steel covers a share of 15% of the total length of the network, while grey cast iron and ductile cast iron have a share of 65% and 20% respectively. The burial depth is assumed equal to 1.5 m for all the pipe segments.

Focusing on the water distribution service, it is fundamental to model the drinking water user demand during time. Time variability of user demand is caused by different factors: climate factors determine variations during the year, the alternation of working and non-working days is responsible for variation during the week and users' activities determine a variation along the hours of the day. This study considers only daily variation of the water demand, which typically shows a main peak in the morning, two secondary peaks in the early afternoon and in the evening and a lower consumption during the night. The typical daily user water demand profile is shown in Fig. 11, normalized by the average node water demand. The average yearly water demand of the district is equal to 314.5 l s$^{-1}$.

Fig. 12 depicts the investigated network layout and shows the average water demand of the nodes. Nodes shown in Fig. 12 may represent tee-junctions, users or water losses. The user water demand is modelled through the time pattern shown in Fig. 11 with a one-minute time step, considering the average daily water demand of that node based on MM database.

### 3.4.3. Solving approach

Once the water network characteristics are fully defined from the hydraulic and the thermal point of view, the next step is represented by the choice of the solving algorithm needed to find mass flow and temperature at each node in the network as a function of time.

Epanet [22] is a public domain software that was specifically coded to model water distribution piping systems. Once the water network is spatially defined (i.e. nodes positions, pipe segment characteristics) and the nodes water demand is set, the software solves the set of non-linear equations that represents the fluid-

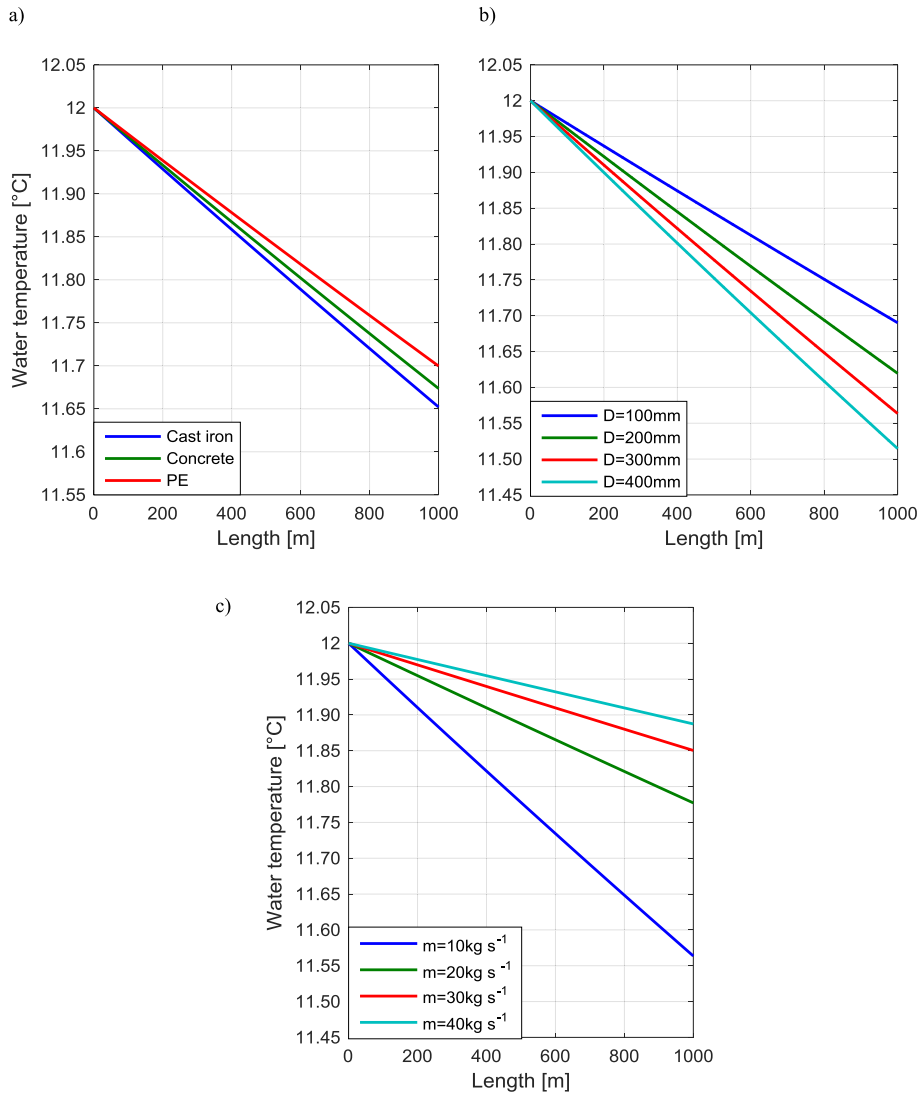


**Fig. 10.** Effect of pipe material (a), pipe diameter (b) and mass flow rate (c) on water temperature profile. Undisturbed soil temperature is equal to 5.71 °C.

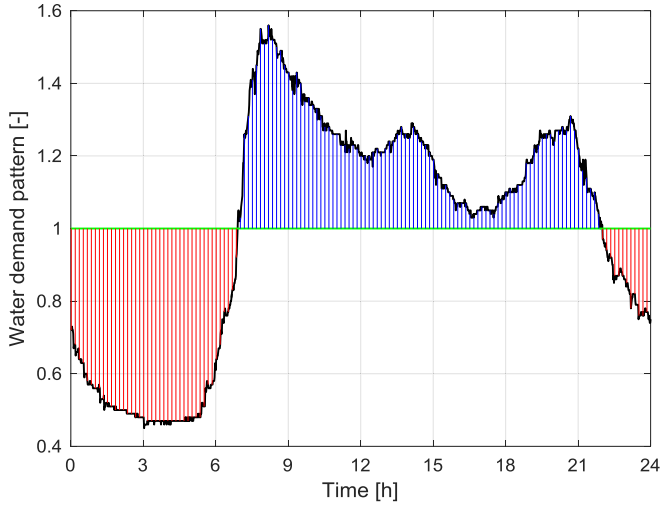


**Fig. 11.** Daily water demand profile (dimensionless) for the Milan network with one-minute time step.

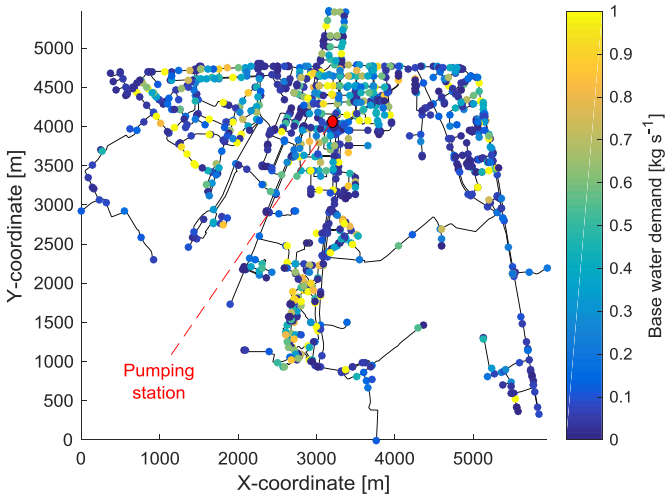


**Fig. 12.** Drinking water distribution network layout, with the pumping station position highlighted. Each node is colored according to its average water demand.

**Table 3**
Monthly thermal load requested for heating. Values are typical of Milan residential users, with a heating period between 15th of October and 15th of April [25].

| User demand | | | |
|---|---|---|---|
| | Days [−] | Monthly thermal energy [kWh m$^{-3}$ month$^{-1}$] | Average thermal power [W m$^{-3}$] |
| October | 17 | 1.39 | 3.41 |
| November | 30 | 6.49 | 9.01 |
| December | 31 | 8.39 | 11.28 |
| January | 31 | 8.39 | 11.28 |
| February | 28 | 7.21 | 10.73 |
| March | 31 | 3.00 | 4.03 |
| April | 15 | 1.39 | 3.41 |

dynamic problem giving as outcomes the mass flow rate and pressure distribution in the network during time. The original Epanet software does not take into account any thermal interaction between the pipe network and the surrounding soil, thus limiting the applicability of this tool for the studied system. Nevertheless, a simple workaround is made available by the usage of the extension package Epanet MSX (Multi-Species eXtension) [23]. This tool is a software extension that was specifically developed to model complex chemical reaction schemes or biological processes that are expressed through a set of differential algebraic equations (DAE); in particular, this package has been originally developed to study the impact on drinking water quality considering processes like formation of disinfection by-products, auto-decomposition of chloramines to ammonia or biological regrowth. In this case, reminding the heat transfer equation of a single pipe in Eq. (20), the temperature can be treated as a concentration term and heat flux as the rate of consumption or generation of the chemical species by chemical reaction, thus allowing the use of Epanet MSX to compute water temperature distribution in drinking water network. It is worth noticing that thermophysical properties of water are assumed to be independent of temperature thus decoupling the thermal problem from the hydraulic problem.

In order to simplify the use of MSX extension, which lacks of a graphical user interface (GUI), a Matlab package [24] that allows operating Epanet within the Matlab environment is used.

It is worth noticing that Epanet considers still water at starting time (t = 0 s). Thus a certain time is needed to reach a steady state condition that represents the real initial condition for time-dependent analysis.

### 3.5. Thermal load

The district heating network served by the heat pump is modelled through a lumped thermal load that represents total energy demand. The thermal demand is influenced by the same factors described for the water demand: climate, users' habits and activities. In this case, seasonal and daily variations of the thermal demand have been considered. In Table 3, monthly thermal energy demands are reported together with average thermal power specific to room volume.

For each month, a representative day (discretized with 1 h time step) is chosen. As an example, the hourly thermal demand of a representative November day, normalized by the nominal HP thermal power (4653 kW$_t$), is shown in Fig. 13.

Similarly to the drinking water consumption, two peaks of heat consumption during the day can be identified. Fig. 13 also shows load conditions where the auxiliary boiler is needed to cover the thermal energy demand. Energy demand higher than the HP design power are characterized by the simultaneous operation of HP and auxiliary boiler, while thermal load below 35% of the HP design power is entirely supplied by the auxiliary boiler.

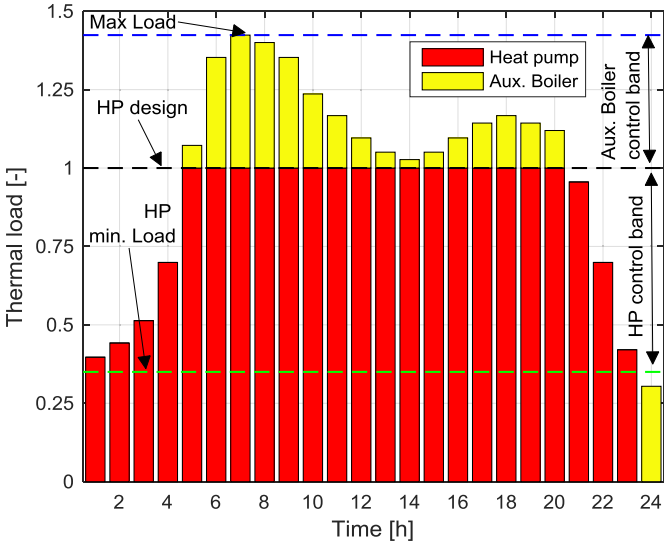


**Fig. 13.** Thermal load profile vs. time for a representative November day. Thermal load is normalized by average thermal power.

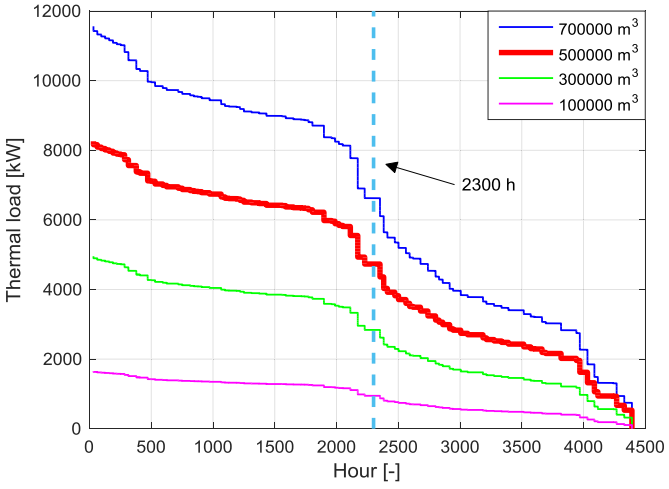


**Fig. 14.** Thermal load duration curve for different total thermal user volumes.

The design load of the HP is defined considering that the district heating network has to serve civil users with a heating volume of 500000 m$^3$, which is of the same order of magnitude of existing district heating systems in Milan. Considering that for economic considerations the HP should work at full load for about 2300 h (this value can be considered as a rough rule derived from authors' experience), a nominal HP power of 4653 kW$_t$ is selected, based on the heat demand curve in Fig. 14. Although the selection of HP size is not derived from a rigorous optimization process based on economic parameter (i.e. payback time, NPV, IRR, etc.), this approach can give a first estimate that can be considered acceptable for the purpose of this study.

The auxiliary boiler is characterized by a nominal capacity of approximately 4000 kW that makes it possible to cover peaks demand. Based on this figure, it is possible to approximately quantify the benefits achievable by the alternative connection in series of the HP and the auxiliary boiler, discussed in Sec. 3.2. At the peak load, the thermal power produced by the entire thermal station would be 8653 kW, 54% of which provided by the heat pump. With a connection in series, the share of the water temperature increase would reflect the power share of the two heating units. Therefore,

of the total 15 °C of temperature increase, 8.1 °C (from 65 °C to 73.1 °C) would be provided by the HP, and the remaining 6.9 °C (from 73.1 °C to 80 °C) by the auxiliary boiler. As a consequence, under this scenario the HP condensing temperature would reduce from the design 82 °C to about 75 °C, with an increase of the COP of about 7%. This represents a non-negligible improvement, but limited to the maximum load conditions. Following the same procedure, it is possible to calculate that for a total thermal load of 6500 kW (which is representative of a significant number of hours in a year, as shown in Fig. 14), the improvement of COP would be of about 5%. On the whole, considering that for half the time the auxiliary heater will not operate, a reduction of the yearly electric consumptions of the order of 2–3% can be expected with a series HP-auxiliary heater connection, with respect to the assumed parallel connection, which does not significantly change the yearly overall energy balance.

In order to understand the difference in size between the district heating and the drinking water customers, it can be considered that the average annual consumption of potable water of a domestic user in Milan is estimated to be equal to 83.1 $m^3$ [26]. Therefore, the drinking water network considered in this study is able to serve approximately 140000 consumers. On the other hand, the total volume of 500000 $m^3$ considered for the district heating users is representative of approximately 5000 users. These values show the significant difference between the number of potable water consumers and associated thermal energy users.

### 3.6. Figures of merit and reference scenarios

The simulation of the drinking water network coupled with the thermal station model produces a set of data of the time-dependent properties of the water in each node and pipe segment (i.e. pressure, mass flow rate, temperature).

As described in the first section, the goal of this study consists in the energetic performance evaluation of the proposed solution of using drinking water as heat source of a district heating system based on heat pump technology. Hence, the definition of the performance indexes plays a fundamental role in evaluating the energy balance of the proposed solution.

In accordance with the simplified analysis proposed in Section 2, the first index is the difference between the primary energy consumption of the two solutions A and B. Primary energy consumption in Case A ($E_A$) is represented by the fossil fuel consumption due to natural gas boilers of the district heating network. It is defined as the ratio between the user thermal load ($Q_{central,NG}$) and the thermal efficiency ($\eta_{th,A}$) as expressed in Eq. (21):

$$E_A = \frac{Q_{central,NG}}{\eta_{th,A}} \tag{21}$$

In Case B, both electric and thermal energy has to be accounted for and converted into primary energy. Focusing on the district heating station, the heat pump is responsible for electricity consumption requested to drive the compressor ($W_{el,compr}$) and the auxiliary heater consumes natural gas to cover thermal demand peaks and part-load operation below the heat pump minimum load threshold ($Q_{aux,NG}$). The electricity is converted into primary energy through a conversion efficiency ($\eta_{el,ref}$) proper of the power production technology demanded to cover the heat pump load, while thermal energy of the auxiliary heater is converted into primary energy through a boiler efficiency $\eta_{th,ref}$. Primary energy and conversion efficiencies are always referred to fuel LHV. Focusing on the end-user, a fraction of the thermal energy extracted from the drinking water by the heat pump ($Q_{RH}$) has to be provided by the end user. This heat corresponds to the energy requested in Case B to reach temperature at node (i) equal to Case A ($T_{i,B} = T_{i,A}$). The reheating heat $Q_{RH}$ at each time step $\Delta t$ (1 min) is computed with Eq. (22), by means of a post-processing procedure, developed in Matlab®, which collects and elaborate all the nodes data derived from Epanet.

$$Q_{RH} = \sum_{i=1}^{N_{user}} \alpha m_i c_{p,water} (T_{i,A} - T_{i,B}) \Delta t \tag{22}$$

The reheating heat is provided by the end user either by electrical heaters ($Q_{RH,EH}$) or by natural gas heaters ($Q_{RH,GH}$), depending on its use as sanitary water or in electrically heated household appliances.

Thus, the primary energy consumption associated with Case B ($E_B$) can be computed as follows:

$$E_B = \frac{W_{el,compr}}{\eta_{el-ref}} + \frac{Q_{aux,NG}}{\eta_{th,B}} + \frac{\frac{Q_{RH,EH}}{\eta_{el,EH}}}{\eta_{el-ref}} + \frac{Q_{RH,GH}}{\eta_{th,GH}} \tag{23}$$

In order to estimate $Q_{RH}$, users' habits about water consumption and usage have to be considered. Table 4 reports the drinking water usage and heated fraction of a typical Italian residential user [27]. From these data, it is possible to compute that 65% ($\alpha$) of the drinking water sent to domestic users needs to be heated. Assuming that the whole thermal load demanded by dish washing and washer is fulfilled by electricity, 46% of drinking water is heated by natural gas boiler while the remaining part (19%) is heated by electric heater. It is worth noticing that electrical boiler is an alternative technology to natural gas boiler. Nevertheless, this option is scarcely adopted in Italian urban context (particularly in Milan) and it is therefore neglected.

Because of the growing interest on global warming and greenhouse effect, a fair comparison between Case A and Case B systems cannot leave out an assessment of carbon dioxide emission. For this reason, specific emission factors have to be assumed for electricity generation ($F_{el}$ [$kg_{CO2}$ $MWh_{el}^{-1}$]) and for natural gas combustion ($F_{NG}$ [$kg_{CO2}$ $MWh_{p}^{-1}$]) respectively.

In agreement with the energy fluxes described above, the $CO_2$ emissions ($e_{CO2}$) for Case A and Case B can be estimated as follows:

$$e_{CO_2,A} = \frac{Q_{central,NG}}{\eta_{th,A}} F_{NG} \tag{24}$$

$$e_{CO_2,B} = E_{el,HP} F_{el} + \frac{Q_{aux,NG}}{\eta_{th,aux}} F_{NG} + \frac{Q_{RH,EH}}{\eta_{el,EH}} F_{el} + \frac{Q_{RH,GH}}{\eta_{th,GH}} F_{NG} \tag{25}$$

As underlined by the definition of the figures of merit, the evaluation of the two investigated solutions is strongly influenced by the assumed conversion efficiencies and emission factors. Central district heating heater in Case A and auxiliary heater in Case B are assumed to have the same conversion efficiency

**Table 4**
Water use of a typical Italian domestic user and fraction of drinking water that requests heating.

| User demand | | |
|---|---|---|
| | Water fraction [–] | Heated fraction [–] |
| Personal hygiene | 0.39 | 0.96 |
| Toilet water | 0.20 | – |
| Wash water | 0.12 | 0.70 |
| Dish washing | 0.10 | 1.00 |
| Cooking | 0.06 | 0.47 |
| Leakage - gardening | 0.06 | – |
| House cleaning | 0.06 | 1.00 |
| Drinking | 0.01 | – |

**Table 5**
Assumptions about the electricity production reference efficiencies and emissions of the three investigated scenarios.

| Assumptions | | | |
|---|---|---|---|
| | Electricity Suppliers [−] | Conversion efficiency [−] | $CO_2$ specific emissions [$kg_{CO2}$ $MWh_{el}^{-1}$] |
| TP | Thermal power plants | 0.446[a] | 555.5[a] |
| CC | Combined cycle | 0.550 | 365.0 |
| RE | Renewable energy | ∞[b] | 0 |

[a] Average efficiency and emissions of Italian thermal power plants.
[b] Reference is made to fossil primary energy consumption.

($\eta_{th,aux} = \eta_{th,B} = 0.90$) and specific $CO_2$ emissions ($F_{NG} = 201$ [$kg_{CO2}$ $MWh_p^{-1}$]). Focusing on the user side, the reduced size of domestic boiler justifies the choice of lower efficiency ($\eta_{el,GH} = 0.85$) while, as regards electric heater, a complete conversion of electricity to heat is assumed ($\eta_{el,EH} = 1$).

With the aim of analyzing the impact of the most uncertain assumptions, three scenarios, which differ in the electricity generation technology that covers the additional electric power demanded by the heat pump and the end users electrical heater, are investigated (Table 5). The first scenario considers a generic thermal fossil fuel plants (TP) as electricity suppliers. Average performance of the Italian power generation fleet has been assumed in this case. The second scenario (CC) considers the combined cycle technology, which is characterized by higher flexibility and typically operates as load-following power plant, which makes it a likely candidate to produce the additional electricity consumed in Case B. Last scenario (RE) considers a condition where only renewable electric energy is used. This option complies with the predictions about future high penetration of intermittent renewable energy sources in the electric energy mix and heat pumps may represent an energy storage and grid service opportunity. Table 5 shows the assumptions that characterize the three considered scenarios.

## 4. Results

Once the model inputs are defined, the described methodology allows computing the behavior of the studied system and returns the system performance indexes. The starting point for technologies comparison is represented by the temperature difference at user nodes between Case A and Case B (see Fig. 15, where solely user nodes are shown). This kind of result is computed for 12 days, each one representative of one month. The figure below represents a condition characterized by a low thermal load that follows a period of high thermal load (as in the initial hours of the day shown in Fig. 13). At such conditions, drinking water mass flow rate processed by the heat pump is low, due to the low thermal load, thus causing a progressive heating of the drinking water. From a qualitative point of view, it is worth noticing that the water temperature difference decreases starting from the heat pump location depending on the water mass flow rate demanded at each node (Fig. 12). The higher the drinking water demand in a node, the faster the water renovation in the pipes bringing the water to that node. For the same reason, some peripheric nodes do not show any difference between Case A and Case B because of very low water demand.

The assesment of the hydraulic behavior, calculating the water mass flow rate at each node, coupled with the calculation of water temperature at each user node, allows computing the reheating energy charged to users and all the energy fluxes in terms of fuel and electricity consumptions. Table 6 reports the characteristic energy fluxes for both the Case A and Case B, namely the energy consumption associated with fuel combustion ($E_{fuel}$), the global electricity consumption ($E_{el}$) and the thermal energy related to heat

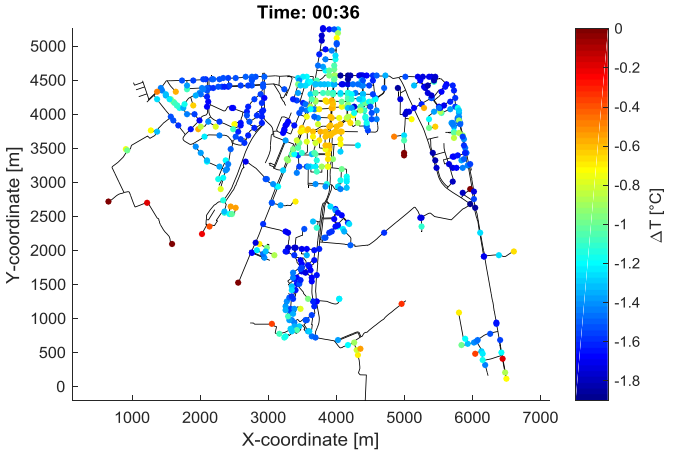


**Fig. 15.** Temperature difference between Case A and Case B at user nodes (November hour: 00:36).

**Table 6**
Monthly and annual energy fluxes for Case A and Case B.

| Energy fluxes | | | | | | |
|---|---|---|---|---|---|---|
| | $E_{fuel}$ [$MWh_p$] | | $E_{el}$ [$MWh_e$] | | $E_{soil}$ [$MWh_p$] | |
| | A | B | A | B | A | B |
| October | 696.2 | 205.5 | 0.0 | 286.2 | −2.6 | 2.7 |
| November | 3244.2 | 1050.7 | – | 1205.4 | −14.5 | −3.5 |
| December | 4196.2 | 1819.1 | – | 1329.1 | −30.3 | −20.5 |
| January | 4196.2 | 1822.6 | – | 1330.6 | −42.8 | −33.3 |
| February | 3606.1 | 1482.4 | – | 1192.9 | −48.5 | −39.1 |
| March | 1500.4 | 492.1 | – | 603.2 | −46.3 | −42.6 |
| April | 614.3 | 196.5 | – | 258.9 | −39.8 | −36.8 |
| Annual | 18053.4 | 7069.1 | – | 6206.3 | −224.3 | −173.1 |

transfer between pipes and soil ($E_{soil}$). With reference to $E_{soil}$ values, negative values are obtained in most of the cases, indicating a heat flow from the water to the colder soil. The only exception is obtained in October for Case B, where the heat pump causes a decrease of the water temperature below the soil one.

With the aim of better understanding reheating energy, the barchart of Fig. 16 shows $E_{RH}$ as a fraction of the total heat $E_{eva}$ extracted by the heat pump evaporator (which corresponds to the total height of the bars). In an extreme situation characterized by both the need of heating the total amount of water mass flow and no heat transfer between soil and water flowing in pipe, reheating energy spent by user would be equal to $E_{EVA}$. Nevertheless, the $E_{RH}$ value is lower than the maximum theoretical one because of three main reasons: i) network leakage flow can be considered as a fraction of cooled water that does not need any further heating,[3] ii) only a fraction $\alpha$ of the user drinking water needs to be heated for

[3] The fraction of water lost in drinking network of Milan is 10.4%. This value is remarkably lower than the Italian average of 31% [28].

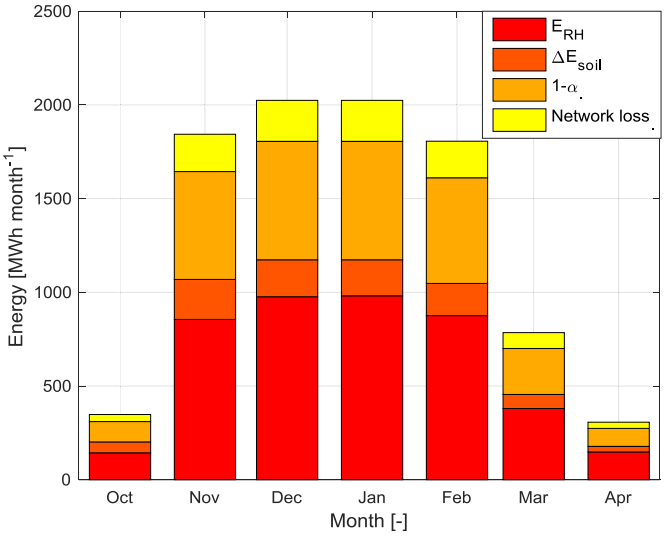


**Fig. 16.** Monthly reheating energy.

the final use and iii) heat transfer from water to soil is reduced by the smaller temperature difference, thus obtaining a sort of energy gain ($\Delta E_{soil}$) that, on annual basis, is equal to 10.3% of the heat extracted by heat pump.

With the aim of comparing Case A and Case B, it is necessary to assess the annual global primary energy consumption computed in accordance with the efficiency assumptions discussed in previous sections. Fig. 17 presents a comparison of the primary energy consumption between Case A and Case B for the three different scenarios shown in Table 5. A breakdown of the energy fluxes related to Case B is also included. It can be noted that taking the generic thermal power plant scenario for electricity generation (TP), the heat pump system leads to augmented consumptions of primary energy. In the CC scenario, the higher electricity conversion efficiency leads to a slight reduction of the primary energy consumption with respect to the scenario of Case A, by about 3–4%. Only the scenario characterized by renewable electricity generation allows fully exploiting the potential of switching from conventional district heating heater to heat pump, with overall fossil primary energy savings of about 60%. It is also worth noticing that consumptions for water reheating represent about 30% (CC scenarios) and 18% (RE scenario) of the total primary energy consumption of the reference Case A.

Fig. 18 shows the carbon dioxide emissions balance that reflects energy balance results presented above. $CO_2$ emission reduction of about 3.5% and 60% can be obtained for fossil fuel power generation and renewable power generation scenario respectively.

## 5. Conclusions and future developments

The use of electrically driven heat pump is recognized as a valuable solution to improve district heating efficiency. It also embodies an opportunity to simplify the management of electric grids in conditions characterized by a high share of renewable energy coupled with energy storage. The present work investigates an integration of a heat pump for district heating in a drinking water network used as the source of thermal energy.

The substitution of a conventional district heating boiler with a heat pump system causes a reduction of the temperature of the water supplied to users, thus involving an additional energy consumption that has to be covered by the user by means of decentralized electric or natural gas heaters. A dedicated model was developed with the aim of considering all the components involved in the energy chain. Epanet coupled with a Matlab® and Thermoflex® were used to perform minute-by-minute simulations of representative days. In order to assess the effect of the adoption of the proposed system on final user, the model is able to predict the temperature of the water supplied to users.

The developed methodology was applied to the case study of a district of the city of Milan. The primary energy consumption and $CO_2$ emissions are calculated and compared with a conventional solution based on a centralized natural gas boiler serving the district heating network.

Specific attention was given to the heat transfer between the water mains and the surrounding soil. The comparison between different thermal modelling approaches identified the Krarti-Kreider's model as the best option in terms of accuracy and computational efforts.

From the simulations, it was found that 10.3% of the annual thermal energy extracted by the heat pump from the drinking water is “recovered” because of the reduced cooling rate of the water in the distribution network. In practice, the water transfers less heat to the colder surrounding soil with respect to the reference case where drinking water is distributed at higher

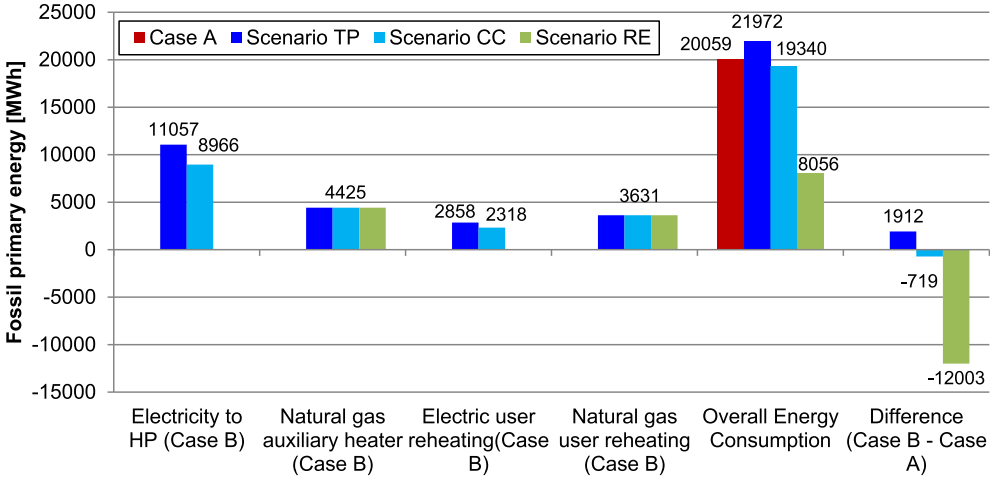


**Fig. 17.** Yearly fossil primary energy balance for the three investigated scenarios. Different shares of primary energy consumption are shown for Case B, while only the consumption of the district heating boiler is considered for Case A.

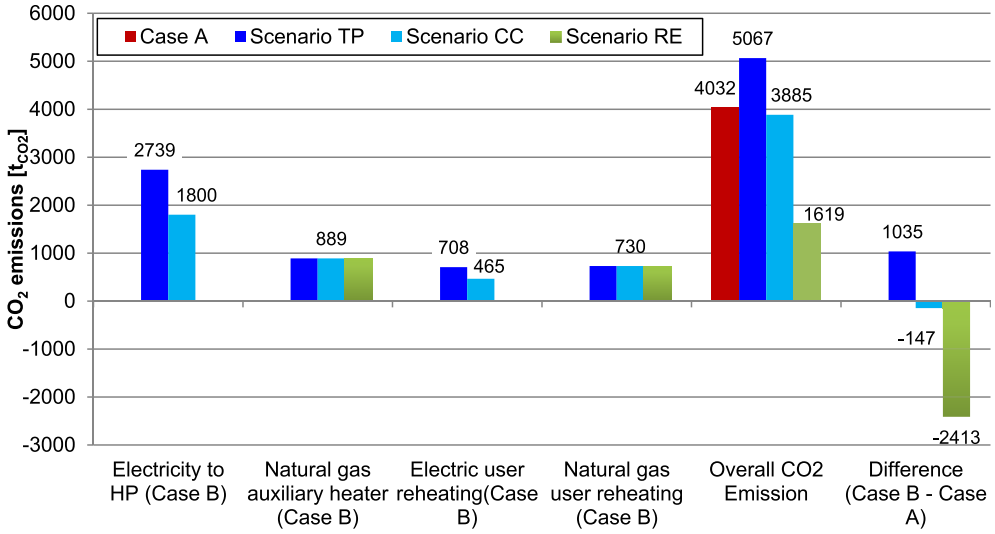


**Fig. 18.** Yearly $CO_2$ emission balance for the three investigated scenarios.

temperature.

Three scenarios are considered to calculate the overall energy balance, characterized by different technologies for power generation. If the electricity to drive the heat pump and for electric heating of potable water is assumed to be produced by a natural gas combined cycle, (CC scenario) a primary energy consumption saving of approximately 3.6% has been obtained. The proposed solution shows all its potential in case electricity is produced by renewable energy technologies (RE scenario). In this case, a reduction of approximately 41% of both primary energy consumption and $CO_2$ emissions can be appreciated and indicates a significant potential of this concept for future electric energy mixes dominated by renewables.

As regards Italy, renewable sources have provided a growing contribution to electricity generation that can be quantified to be equal to 33% (related to 2015) [29], hence, the reduction of primary energy, which can be reached through the adoption of the proposed system, is approximately 13.5%.

It is worth underlining that energy efficiency can be increased by the adoption of low temperature heat pump technology, which is characterized by a higher COP, that requests the adoption of low temperature heating technologies (e.g. underfloor heating system, fan coils etc.). Although not feasible for existing buildings, this represents a promising solution that is worth being considered for new municipal districts.

With the aim of increasing the accuracy of the model, future developments could be addressed towards the inclusion of a more accurate modelling of user heat demand, which is affected by external parameters (i.e. hourly ambient temperature, user habits, HVAC control etc.), and the thermal behavior of buildings.

Finally, it is worth highlighting that to identify the best solution to integrate drinking water with district heating networks and make the proposed system more attractive, rigorous optimization routines may be employed, to optimize both the components design and the control strategy.

## Appendix. Soil temperature calculation model

Soil temperature plays a fundamental role in the prediction of the heat transfer between a buried pipe and the surrounding soil. A common approach approximates the soil as a semi-infinite medium whose free surface temperature varies according to a sinusoidal function as expressed in the following relation [30]:

$$T_{amb}(t) = T_m - A\,cos[\omega(t+S)] \tag{26}$$

where $T_m$ is the mean value, $\omega$ the wave pulsation and S the time offset.

In order to identify the sinusoidal function parameters, ambient air temperature, which is assumed to approximate the free surface ground temperature, is taken from the Energy Plus database [31], sampled with one hour time step. Weather data are processed with a least-square method to compute the sinusoidal function that is then used in the model.

Fig. 19 shows the ambient temperature data for Milan [31], distinguishing the original data, the mean daily temperature and the sinusoidal approximation.

The problem of computing the soil temperature profile at a depth y in a time of the year t can be solved analytically assuming heat conduction in a semi-infinite solid with imposed sinusoidal

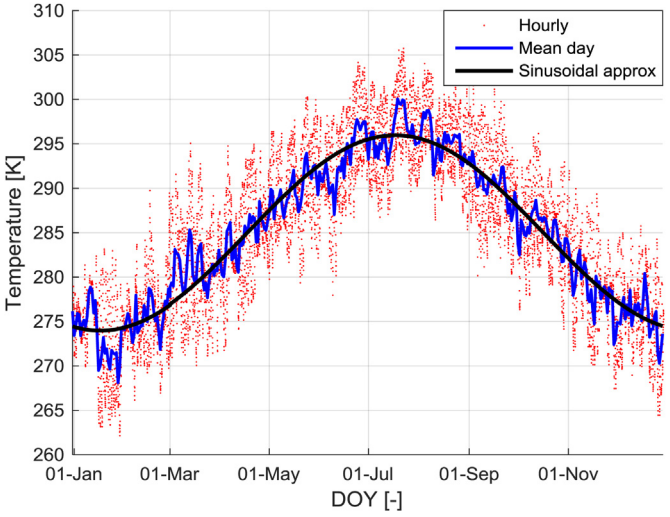


**Fig. 19.** Hourly sampled ambient temperature taken from Milan weather data [31] (red-dotted), mean daily ambient temperature (blue) and sinusoidal function best fit (black). (For interpretation of the references to colour in this figure legend, the reader is referred to the web version of this article.)

**Table 7**
Parameters used in Eq. (27) for the calculation of the soil temperature.

| Reference case layout | | | |
|---|---|---|---|
| | Symbol | Value | Unit of Measurement |
| Mean temperature | $T_m$ | 11.81 | °C |
| Amplitude | A | −11.00 | °C |
| Time Offset | S | −17.08 | day |
| Angular frequency | ω | 1.9924E-07 | $s^{-1}$ |
| Soil thermal diffusivity | α | 6.48e-7 | $m^2\ s^{-1}$ |

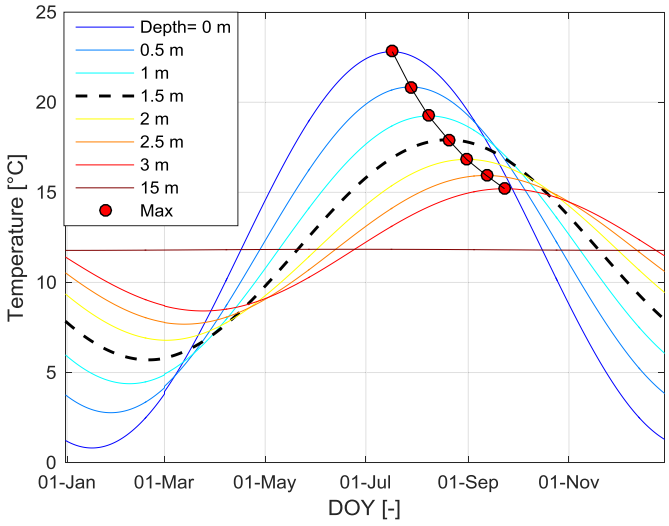


**Fig. 20.** Soil temperature profile for different burying depths.

surface temperature (Eq. (26)). The result is described by the following sinusoidal function [16]:

$$T(y,t) = T_m + Ae^{\left(-\sqrt{\left(\frac{\omega}{2\alpha}\right)}y\right)} cos\left[\omega(t+S) - \sqrt{\left(\frac{\omega}{2\alpha}\right)}y\right] \qquad (27)$$

Table 7 summarizes the parameters used to compute the soil temperature profile.

Fig. 20 shows the annual soil temperature profile at different depths computed with Eq. (27). An increase of the burial depth entails a reduction of the amplitude of temperature oscillation and an increase of the time offset (delay). It is worth noticing that soil temperature remains undisturbed at high depth (e.g. at 15 m depth).

## References


[1] Intergovernmental Panel on Climate Change, Intergovernmental Panel on Climate Change (IPCC), http://www.ipcc.ch/, 2015 (2013).
[2] Satterthwaite D. Cities' contribution to global warming: notes on the allocation of greenhouse gas emissions. Environ Urban 2008;20(2):539–49.
[3] Rosenzweig C, Solecki W, Hammer SA, Mehrotra S. Cities lead the way in climate-change action. Nature 2010;467(7318):909–11.
[4] Heat pump centre. Heat pumps- A key technology for the future. Heat Pumps Smart Grids Smart Cities 2012;30.
[5] Di Domenico S. Analisi delle fognature e relative applicazioni energetiche [Master Thesis]. Alma Mater Studiorum - Università degli studi di Bologna, Dipartimento di Ingegneria delle Strutture dei Trasporti, delle Acque, del Rilevamento, del Territorio; 2010.
[6] Frijns J, Hofman J, Nederlof M. The potential of (waste)water as energy carrier. Energy Convers Manag 2013;65(0):357–63.
[7] Elías-Maxil JA, van der Hoek JP, Hofman J, Rietveld L. Energy in the urban water cycle: actions to reduce the total expenditure of fossil fuels with emphasis on heat reclamation from urban water. Renew Sustain Energy Rev 2014;30:808–20.
[8] Wiltshire R. Advanced district heating and cooling (DHC) systems. Woodhead Publishing; 2015.
[9] Fiore S, Genon G. Heat recovery from municipal wastewater: evaluation and proposals. Environ Eng Manag J 2014;13(7):1595–604.
[10] Friotherm. Friotherm: unitop product. 2015. http://www.friotherm.com/en/products/unitop/.
[11] Thermoflow Inc.. Thermoflex v.24 user guide. 2014. https://www.thermoflow.com/.
[12] Kreith F, Wang SK, Norton P. Air conditioning and refrigeration engineering. CRC Press; 1999.
[13] Farouki OT. The thermal properties of soils in cold regions. Cold Reg Sci Technol 1981;5(1):67–75.
[14] Barletta A, Lazzari S, Zanchini E, Terenzi A. Transient heat transfer from an offshore buried pipeline during start-up working conditions. Heat Transf Eng 2008;29(11):942–9.
[15] Multiphysics modeling and simulation software (COMSOL). 2012. http://www.comsol.com/.
[16] Bergman TL, Incropera FP, Lavine AS, DeWitt DP. Fundamentals of heat and mass transfer. Wiley; 2011.
[17] Blokker EJM, Pieterse-Quirijns EJ. Modeling temperature in the drinking water distribution system. J Am Water Works Assoc 2013;105(1):35–6.
[18] Blokker EJM, van Osch AM, Hogeveen R, Mudde C. Thermal energy from drinking water and cost benefit analysis for an entire city. J Water Clim Change 2013;4(1):11–6.
[19] Bejan A, Kraus AD. Heat transfer handbook. New York: J. Wiley; 2003.
[20] Krarti M, Kreider JF. Analytical model for heat transfer in an underground air tunnel. Energy Convers Manag 1996;37(10):1561–74.
[21] MacAller SA. Potential for heat recovery from danish drinking water supply [Master Thesis]. Technical University of Denmark (DTU) - Environmental Engineering; 2013.
[22] Rossman LA. EPANET 2: users manual. US Environmental Protection Agency. Office of Research and Development. National Risk Management Research Laboratory; 2000.
[23] Shang F, Uber JG, Rossman LA. EPANET multi-species extension user's manual. Cincinnati, Ohio: Risk Reduction Engineering Laboratory, US Environmental Protection Agency; 2008.
[24] Kyriakou M, Eliades D. EPANET-Matlab-ClassA: Matlab class for EPANET water distribution simulation libraries. 2014. https://github.com/KIOS-Research/EPANET-Matlab-Class.
[25] Colombo M, Camusi M, Saracino M. Teleriscaldamento associato a pompa di calore. Un esempio a Milano: la Centrale di Canavese. 2005.
[26] ISTAT. Water rationing and consumption for domestic use for the provincial capitals [Indicatori sull'acqua per uso domestico per i comuni capoluogo di provincia] (in Italian). 2011. p. 2015. http://dati.istat.it/Index.aspx?DataSetCode=DCCV_INDACQDOM.
[27] Altroconsumo. Acqua, come evitare gli sprechi. Altroconsumo 2014;283.
[28] Metropolitana Milanese. Milan drinking water system. 2016 (in Italian), http://www.metropolitanamilanese.it/pub/page/it/MM/acquedotto_distribuzione.
[29] Gestore Servizi Energetici. Energia da fonti rinnovabili in Italia. 2016 (in Italian), http://www.gse.it/it/Statistiche/RapportiStatistici/Pagine/default.aspx.
[30] Hillel Daniel. Introduction to soil physics. New York: Academic Press; 1982.
[31] EnergyPlus. EnergyPlus energy simulation software: weather data. 2012. http://apps1.eere.energy.gov/buildings/energyplus/weatherdata_about.cfm.